664512

DP-906

AEC RESEARCH AND DEVELOPMENT REPORT

MICROPROBE STUDY OF ZIRCALOY CORROSION FILMS

Kurt F. J. Heinrich

DUPONT
REG. U. S. PAT. OFF.

ISSUED BY

Savannah River Laboratory

Aiken, South Carolina

LEGAL NOTICE

Printed in USA. Price $2.00
Available from the Clearinghouse for Federal Scientific and Technical Information, National Bureau of Standards, U. S. Department of Commerce, Springfield, Virginia

664512

DP-906

Metals, Ceramics, and Materials
(TID-4500, 34th Ed.)

MICROPROBE STUDY OF ZIRCALOY CORROSION FILMS

by

Kurt F. J. Heinrich
Pigments Department

Approved by

W. B. DeLong, Section Director
Technical Division, Reactor Materials

November 1964

E. I. DU PONT DE NEMOURS & COMPANY
SAVANNAH RIVER LABORATORY
AIKEN, SOUTH CAROLINA

CONTRACT AT(07-2)-1 WITH THE
UNITED STATES ATOMIC ENERGY COMMISSION

ABSTRACT

The primary object of this study was to determine the potential usefulness of the electron probe analyzer as a tool for the investigation and elucidation of problems in the corrosion of zirconium alloys, particularly Zircaloy-2.

The general applicability of the probe to corrosion studies was demonstrated. Techniques were developed for the preparation and study of corroded zirconium alloy specimens. Previously unknown characteristics of the distribution of the component elements were revealed in Zircaloy-2 specimens and other zirconium alloys which had been subjected to various heat treatments. Data were also obtained on the composition and distribution of alloy elements in the fundamental corrosion layers.

The possible significance of these findings is discussed in the light of current theories on corrosion mechanisms in zirconium alloys.

CONTENTS

LIST OF FIGURES

LIST OF TABLES

MICROPROBE STUDY OF ZIRCALOY CORROSION FILMS

INTRODUCTION

The alloy Zircaloy-2 (Zr-2)[a] has been developed for use as a fuel cladding and structural material in water-cooled nuclear reactors. Strength in the alloy is achieved by the addition of tin, while corrosion resistance is enhanced by the use of iron, chromium, and nickel. This alloy is being used successfully up to coolant temperatures of about 300°C, but corrosion and hydriding generally do not permit its use at substantially higher temperatures.

Higher operating temperatures would increase the efficiency of these reactors. An understanding of the corrosion mechanism is necessary in order to develop zirconium alloys capable of higher temperature operation.

The principal purpose of this work was to establish whether the electron microprobe could provide useful information on the microchemistry of the oxide film and underlying metal. If the microprobe was deemed useful for this type of work, it was hoped that the distribution of alloying elements could be determined and some light shed upon the relationship between the microchemistry of these alloys and their observed corrosion behavior.

SUMMARY

It was established that the spatial resolution and analytical sensitivity of the Electron Probe Microanalyzer can be applied to the investigation of the distribution of alloying elements in zirconium alloys and in their corrosion products.

In alpha-annealed Zr-2, the chromium and nickel segregate in discrete islands; iron enrichment is found in both segregates and only in these areas. The concentrations of iron, chromium, and nickel in the matrix (nonenriched areas) of the alloy were determined. In thick oxide films (typical of posttransition corrosion), similar areas of iron-chromium enrichment were identified; those involving iron-nickel were fewer in number and less highly enriched in the oxide than in the metal matrix. Tin was distributed uniformly in both the metal and in the oxide.

(a) Nominal composition - 1.45% Sn, 0.135% Fe, 0.10% Cr, and 0.055% Ni.

In preliminary examinations of Zr - 1 wt % Ni, and Zr - 2.5 wt % Nb - 0.5 wt % Cu, local enrichment of the alloying elements was not observed.

Stringers of white oxide on the surface of autoclaved Zr-2 contained high iron concentrations — higher than would be expected for any normal structural feature of the alloy. Insufficient work was done to define the origin of such surface defects.

EQUIPMENT AND EXPERIMENTAL TECHNIQUES

A. Electron Microprobe Technique

The electron probe microanalyzer is an X-ray emission spectrograph in which X-rays emitted from a microscopic area of the specimen are analyzed to determine the composition of the area. This is achieved by bombarding the specimen with a focused beam of accelerated electrons and then analyzing the X-rays emitted from the excited area. The instrument is unique in that it permits the equivalent of a chemical analysis to be made of a solid volume of 1 to 10 cubic microns. Hence, metallographic observation of an alloy specimen can be complemented by characterizing the composition of inclusions, diffusion gradients, oxidation zones, and areas near grain boundaries.

The instrument used is an EMX Scanning Electron Microprobe X-ray Analyzer made by The Applied Research Laboratories of Glendale, California. It is capable of bombarding specimens up to 1 inch in diameter with an electron beam of less than 0.5 μ diameter. Under these conditions the X-rays are emitted from a volume 1 to 3 μ in diameter. The accelerating voltage may vary from 1 to 50 kev. The characteristic X-rays emitted by the elements composing the sample are analyzed by three X-ray spectrometers. These spectrometers, which may be operated simultaneously, cover a wave length range of 1 to 10 Å*, so that elements with an atomic number greater than 11 may be detected and analyzed. The sensitivity of this instrument permits maintaining the beam current below 2.5×10^{-8} ampere. This minimizes the problems of overheating and electrostatic disturbances while still maintaining a satisfactory intensity of X-ray output.

A reflecting light microscope permits direct visual observation of the specimen under the electron beam. Mechanical and electronic scanning attachments allow the following modes of analysis:

---

* In this study the Kα lines were used for Cr, Cu, Fe, and Ni, and the Lα lines for Nb, Sn, and Zr.

1. Quantitative analysis of a small region, 1-3 μ in diameter and depth. The beam is held stationary and the X-ray photons emitted by the element of interest are counted. The limit of detection by this technique for most alloying elements encountered in this study was about 100 ppm.

2. Quantitative analysis of larger area region: approximately 1200 square microns. The beam is rapidly scanned over the same area while the X-ray photons of interest are counted.

3. Semiquantitative analysis along a line across the specimen; the readout was registered on a chart recorder.

4. Qualitative scans over an area of the specimen. In area scans the X-ray signals represent alloy element distribution. Target current and backscatter images show topographic features and differences in average atomic number.

B. Specimen Preparation

The first transverse sections of corroded Zr-2 mounted in bakelite showed the following defects (Figure 1-a):

- Excessive rounding of the specimen edges.
- Shrinkage of the mounting medium adjacent to the specimen.
- Frequent shattering and partial loss of the oxide coating.

Better results were obtained by using diallylphthalate as a mounting medium, and by close juxtaposition of the specimens to avoid rounding in polishing (Figure 1-b). The specimens were then polished on wet silicon carbide papers, up to 600-grit, and finished with 12-, 6-, and 1/4-micron diamond compound. Chemical etching was avoided to eliminate preferential etching of alloying elements in the specimen.

Electron microprobe analysis requires adequate electrical and thermal conductivity of the specimen surface. Electron bombardment of Zircaloy specimens having oxide films of low electrical conductivity results in instability of beam position due to formation of electrostatic charges on the sample surface. This was eliminated by vacuum evaporation of a thin layer of aluminum onto the surface of the mounted and polished specimen. Comparison of uncoated and aluminized standards (Figure 2) showed that the aluminum coatings, while eliminating the formation of electrostatic fields, were sufficiently transparent to both electrons and X-rays as not to interfere with the analytical procedures.

C. Bulk and Matrix Analysis of Alloying Elements

One of the early experiments performed in this work was the evaluation of the microprobe as an analytical tool for the determination of the concentration of the normal alloying elements in zirconium alloys similar to Zircaloy-2 on both a bulk and micro scale. Three "standard" samples were obtained from U. S. Industrial Chemicals Co. These specimens were irradiated by adjusting the electron beam so as to scan an area of 1150 square microns, which area is sufficiently large to overlap the normal microstructural constituents. The characteristic line emissions of the tin L alpha, and the K alpha lines of Fe, Cr, and Ni were thus measured for a number of sample areas at random.

Figure 3 illustrates the calibration curves obtained by plotting the average counting rate against the concentrations as determined by standard analytical methods. Although the relationship is linear for the range covered, the counting rate does not extrapolate to zero at zero concentration as a result of background. Table I compares the actual values reported by the manufacturer for the individual standards with the values obtained from the linear calibration curves.

These calibration curves could also be employed to measure the concentration of the alloying elements in the matrix. For this purpose, analogous measurements were taken with a static beam of diameter smaller than one micron.

RESULTS

A. Zircaloy-2

The Zircaloy-2 specimens used in this study are described in Table II. The autoclaved sheet specimens were supplied by the Atomic Energy of Canada, Ltd. (AECL) and the Bettis Atomic Power Laboratory (BAPL). Ingot analyses for two of the AECL specimens are shown in Table III. The Zircaloy-2 samples had been etched in the normal $HF-HNO_3-H_2O$ solution, rinsed and exposed in steam (400°C) or water (360°C and lower) autoclaves under the conditions listed in Table II. The resulting corrosion film weight gains are also listed. The analyses for the alloying elements, as obtained by the microprobe, are included in Table II. In spite of the differences of distribution of the alloying elements in these specimens, the analytical data obtained by the microprobe are fairly comparable (Specimens J-3930, J-3932, J-3960, and L-1195).

1. Microprobe Results on Metal Portions of Samples

a. Alpha-Annealed Specimens

Area scans of alpha-annealed specimens from both sources are shown in Figures 4 and 5. In X-ray area scans, light areas represent those regions where the alloying element of interest is concentrated. Iron, chromium, and nickel are shown to be highly segregated, with local concentrations considerably higher than the over-all concentration. (Part of the gray tone observed in Figures 4-c,d,e between zones of high concentration is due to X-ray background from continuous radiation (Bremsstrahlung) rather than the residual concentration of the alloying elements.) These areas of high concentration are 1 to 3 μ in diameter and roughly circular in shape. In some specimens, they are arranged in a netlike fashion with an average distance across openings in the net about one grain diameter (see Figures 5-c and d). This suggests that in some cases the areas of high concentration may be located preferentially at grain boundaries.

In general, these area scans do not reveal any marked variation in tin concentration. Occasionally, tin does appear to be slightly depleted in the areas of higher concentration of the other alloying elements (see Figure 5-e). However, there were no areas of pronounced increases in tin concentration.

Close comparison of the scans for different elements in the same area of the specimen shows that there are two types of association of alloying elements (see Figures 4-c and e). The first is characterized by high levels of iron and chromium, and the second by iron and nickel. There were no other concentrations of either a single element or combinations of elements. These local regions of high concentration were grouped together with relatively wide spaces separating the groups.

Line scans within the metallic part of the specimen confirm the observations made on area scans. Figure 6 shows such line scans on a typical sample. The following observations can be made:

- The iron-nickel association is clearly indicated in Figures 6-a and b (points marked A), as well as the iron-chromium association (points marked B). Furthermore, in no case are iron concentrations observed without corresponding increases in chromium or nickel.

- In areas other than those corresponding to the above mentioned associations, the levels of chromium, nickel, and iron are quite close to the zero (background) level, marked at the side of the graphs.

- The tin concentration is slightly depleted in regions in and adjacent to those areas of concentrations of iron-chromium and iron-nickel (Figures 6-c and d). In no case, however, does the tin concentration drop to zero in these areas.

Attempts were made to quantitatively analyze the composition of the highly segregated areas by point-counting with a stationary beam. Alloy contents of several percent were indicated in both types of associations; however, the accuracy of the data obtained is doubtful due to the small size of most particles relative to the volume of metal analyzed.

It was, however, possible to analyze the concentration of alloying elements in the "matrix" of the metal (ie, in areas that do not show enrichment). The results obtained in four regions of one specimen are given in Table IV. The concentrations of iron, chromium, and nickel in the matrix of this sample are 60-80% lower than their nominal concentrations.

b. Specimen Annealed in the Alpha + Beta Region

Area scans obtained on the specimen annealed in the alpha + beta phase region are shown in Figure 7. The element distribution differs from that of the alpha-annealed specimens in that

1) Areas enriched in iron, nickel, and chromium are distributed in a coarser fashion.

2) Iron and chromium distributions match exactly. Nickel appears in areas where iron and chromium are most heavily concentrated.

3) The iron-chromium distribution has a more clearly defined netlike appearance.

4) Tin depletion in the enriched areas is more pronounced.

c. Beta Heat-Treated Specimens

Several specimens heat treated in the beta region were examined (Figures 8 and 9). As in the alpha + beta treated specimens, the distributions of iron and chromium are coincidental, while nickel is enriched in a less connected pattern in the areas of highest iron and chromium concentration. Unlike the alpha or alpha + beta treated material, these specimens show alloying elements deposited in parallel bands, suggesting distribution between the lamellae of a Widmanstatten structure. The tin depletion within these bands is very pronounced, probably complete (Figure 8-d). In the beta-annealed specimens, the dimensions of areas free of alloying element enrichment were considerably larger than in alpha-annealed specimens (compare Figures 4-c and 8-a). The bands rich in iron, nickel, and chromium are those regions transformed last from the beta phase to the alpha phase during cooling. In the beta-quenched specimens (Figure 9), the lamellae between the alloy concentration bands are thinner, and the alloy content in the lamellae is higher. Presumably the faster cooling of these specimens did not permit as distinct a segregation of the alloying elements.

2. Microprobe Results on Oxide Films

a. Transverse Specimen Sections

Limited data were obtained on the distribution of the alloying elements in the corrosion film on the Zr-2 specimens. Data came from oxide films more than 5 μ thick. The film thickness is indicative of posttransition corrosion, when the weight gain becomes approximately linear with time.

Line scans through a limited number of Zr-2 corrosion films (Figure 10) indicated that the alloy element distribution in the oxide differs from that in the metal. Although the frequency and height of the iron-chromium aggregates are similar to those in the metal, the iron-nickel concentrations are diminished both in frequency and concentration. Consistent with this, the chromium content of the oxide matrix is as low as it is in the metal, while the concentrations of nickel and particularly iron in the oxide matrix are considerably higher. Obviously, the iron-chromium association in the metal is conserved in the oxidation process, while the iron-nickel association is either finely dispersed in the oxide, or, most probably, dissolved.

Repeated examination of the metal-oxide interface showed no enrichment of any of the alloying elements at or near the interface. This could be significant in view of the different behavior of the two other alloy systems described below.

A limited number of point counts on thick oxide coatings indicated that statistically meaningful analytical results can be obtained; hence, quantitative analysis of the oxide coatings is possible. However, the data were insufficient to draw quantitative conclusions as to oxide film composition.

b. Observations on Stringers

An attempt was made to determine the nature of stringer-like defects in the oxide film of certain specimens. This type of defect is mentioned frequently in the literature and is usually associated with stringer-like defects in the metal.

Microscopic examination of the oxide stringers shows elongated areas of white corrosion film in the work direction of the specimen. In many instances the white oxide is bulged or broken away from the specimen surface (Figure 11-a).

Several stringers were examined with the microprobe. Because of the difficulty in accurately locating them in transverse cuts, the unprepared specimen surface was examined directly. Every stringer examined showed areas of high iron concentration, but only where the oxide had broken away from the specimen (Figures 11-b and 12). There were no iron-rich areas in the oxide film between stringers. They were significantly larger than the iron-rich regions in the metal, and were not associated with the presence of either chromium or nickel. Because the iron distribution pattern was so different from that normally found in the bulk of the metal or oxide, it is not likely that these iron-rich areas are a normal feature of the alloy. Data were insufficient to determine whether these iron-rich regions were deposited in the specimen surface during fabrication or corrosion. Hence, it was not possible to determine the role of these regions in the formation of the oxide stringers.

B. Zirconium–2.5 wt % Niobium–0.5 wt % Copper

A series of Zr-Nb-Cu alloys, with chemical analyses as shown in Table III, were supplied by AECL for this study. Some samples were annealed for 1 hour at 850°C (in the alpha + beta region) and furnace-cooled; others were solution-treated in the beta region for 15 minutes at 960°C, quenched in water, and tempered at 500°C for 24 hours. The specimens were then exposed at atmospheric pressure to replenished carbon dioxide at 475°C maintained at a dew point of 10°C. Each specimen was exposed for 67 days. The typical weight gains for the two groups were 540 mg/dm^2 and 250 mg/dm^2, respectively.

Two specimens of this composition, one of each heat treatment, were examined by area and line scans. The first specimen (B-246) had been beta-quenched and tempered and exhibited the lower weight gains. Typical line scans across the metal and into the oxide are shown in Figure 13. These data show that niobium and copper are homogeneously distributed within the metal, within the sensitivity of the scanning procedure. At the metal-oxide interface the copper concentration is enriched to a level 50% above the average concentration in the metal. The niobium shows no such accumulation at that point. Both the copper and niobium are rather homogeneously distributed in the oxide. The niobium concentration (relative to zirconium) in the oxide film is the same as in the metal; however, the copper concentration appears to be less by about 20%. This is consistent with the copper accumulation at the metal-oxide interface.

The second specimen of this alloy (B-179), which had been annealed in the alpha + beta region, exhibited relatively poor corrosion resistance. A typical transverse scan across the metal and into the oxide film is shown in Figure 14. Both the niobium and copper fluctuate in the metal to a greater degree than in the beta-quenched specimen. This fluctuation amounts to about ±10% for niobium, and about ±20% for copper. There is no apparent accumulation of either copper or niobium at the metal-oxide interface. Niobium is fairly homogeneously distributed in the oxide film. In contrast, the copper was inhomogeneously distributed in the oxide and had peaks in concentration far above the average composition.

C. Zirconium–1 wt % Nickel

A single specimen of Zr - 1 wt % Ni was analyzed to aid in determining the effect of abnormally high concentrations of one alloying element in zirconium on the chemistry of the corrosion film. This specimen, obtained from Nuclear Metals, Inc., was spherical and had been quenched from the beta phase region (950°C). It had been subsequently autoclaved for 165 hours in 600°C steam; the resulting weight gain was 150 mg/dm^2.

Figures 15 and 16 show typical area and line scans. In the area scan of the metal portion, the nickel was strongly segregated, with a low but detectable concentration between areas of high nickel content. Both the area and the line scans show a significant increase in nickel content at the metal-oxide interface. The nickel was evenly distributed at a low concentration within the oxide. The level of this concentration was not measured. However, in view of the accumulation of nickel at the metal-oxide interface, the concentration of nickel in the oxide is less than 1%.

DISCUSSION

It was the purpose of this work to establish the extent to which the distribution of alloying elements in zirconium alloys and in their oxide films could be determined with the electron microprobe. It was hoped that the observations of alloy element distribution in the corrosion films would contribute to an understanding of the corrosion process.

The results indicate that the electron microprobe has sufficient spatial resolution to reveal, in area and line scans, characteristics of the distribution of alloying elements (not been previously documented) that vary with the

heat treatment the specimen had been subjected to. The instrument was sufficiently sensitive to determine, with stationary beam techniques, the concentration of alloying elements at the lowest levels encountered (ie, in the matrix and within thick oxide layers). Hence, both the type of distribution and the residual levels of alloying elements in specimens of varying histories can be determined and correlated with measured corrosion resistance characteristics.

Data obtained by the microprobe during this study are in two categories: analyses of the metal portion of the corroded samples, and analyses of the corrosion films themselves. Each of these is discussed below.

A. Alloying Elements in the Metal

Data obtained on the metallic portion of the corroded samples were consistent with the published phase relationships[1] for the zirconium alloys used in this study. In Zr-2 specimens the material slow-cooled from the beta phase showed gross accumulation of alloying elements in a netlike pattern. These areas were enriched in iron, chromium, and nickel and were depleted in tin. This behavior has been predicted from phase relationships which show that iron, nickel, and chromium are more soluble in the beta phase than in the alpha and that the reverse is true for tin.[2] Hence, as the alloy cools, the former three elements are expected to be retained in the diminishing beta phase while the tin should be confined principally to the growing alpha phase. The bands rich in iron, nickel, and chromium thus represent the last of the beta phase to transform to the alpha phase during the cooling process. Although this behavior has been predicted previously, to the author's knowledge this is the first published detailed documentation of the partitioning effect.(a)

Similar partitioning effects were noted in the Zr - 1 wt % Ni alloy also cooled from the beta phase. The samples of Zr-2 that were quenched (rather than slow-cooled) from the beta phase showed a more diffuse distribution of iron, nickel, and chromium around a Widmanstätten structure. This broader distribution of alloying elements is presumably due to the more rapid cooling through the beta and high-alpha phases.

(a) A microprobe study by Oestberg[3] and a brief note by Kirianenko and Maurice[4] are in substantial agreement with our observations.

In the metal portion of the beta-quenched and tempered Zr-Nb-Cu alloys, the niobium and copper was quite homogeneously distributed. Dalgaard[5] has shown that the Zr - 2.5 wt % Nb alloy in the beta-quenched and tempered condition contains a very fine precipitate with an interparticle spacing of only 0.1 to 0.2 μ. A similar distribution may be expected in the copper-bearing alloy, because both the niobium and the copper in the amounts present are readily soluble in the beta phase, but insoluble in the alpha. Hence, beta treatment would result in dissolution of the alloying elements, and little or no precipitate would form during subsequent water quenching. However, on tempering at 500°C, part of the niobium and most of the copper would precipitate, presumably as very fine particles, as in the case of Zr - 2.5 wt % Nb alloys. If the interparticle spacing in the copper-bearing alloy is similar to that of the Zr-Nb alloy, the presence of such fine particles in the matrix would not necessarily be detected by the microprobe analyzer.

The microprobe results also indicated that in the beta-treated, slow-cooled Zr-Nb-Cu alloy the niobium and copper fluctuations were considerably greater than in the quenched and tempered sample. This is consistent with the solubility data discussed above, because slow-cooling from the beta phase would result in a more coarse Nb-Cu-rich precipitate.

B. Alloying Elements and the Corrosion Process

The role of alloying elements in the corrosion process has been investigated. Britton and Wanklyn[6] viewed the role as principally mechanical, and suggested that the intermetallic compounds in the metal might exert a "keying" effect in the oxide, preventing propagation of oxide film cracks and subsequent film breakdown. Cox[7] compared the oxidation of sponge zirconium and Zr-2 and concluded that the fine dispersion of intermetallics in Zr-2 persisted in some form in the oxide. He postulated that this population of intermetallics would promote a more uniform diffusion of oxygen through the film (resulting in a more even oxide growth pattern), and hence postpone film breakdown.

Others have suggested that the alloying elements should be dissolved in the oxide to be influential in controlling corrosion. Tin should be dissolved in the oxide, in order to counteract the detrimental effect of nitrogen on the corrosion of zirconium. Dalgaard pointed out that the copper in a Zr - 2.5 wt % Nb - 0.5 wt % Cu alloy enhances the corrosion resistance only when it is distributed in the metal so that a homogeneous distribution is possible in the oxide. In previous work, there was no evidence of copper in the oxide.

This present work demonstrated that some alloying elements of the metal are indeed homogeneously dispersed in the corroding film, within the limit of the resolution of the microprobe analyzer. The significance of this and other findings is discussed below.

1. Zircaloy-2

The oxidation of zirconium involves the diffusion of oxygen ions through the oxide film to the oxide-metal interface. At this point the reaction with zirconium takes place, building up oxide underneath the existing layer. The rate of oxygen ion diffusion toward the metal will depend upon the flow of vacancies in the opposite direction. The vacancies would be oxygen ion vacancies because of the ionic radii and because the oxide is initially depleted in oxygen. Hence, the addition of any metal ion to the oxide film which will decrease the concentration of oxygen ion vacancies will tend to decrease the corrosion rate. Thus, pentavalent and hexavalent cations substituting in Zr + 4 sites or interstitial cations of any valence will add electrons to the oxide lattice and decrease the number of oxygen ion vacancies so that the corrosion rate would be reduced. On the other hand, substitution of a divalent or trivalent cation for Zr + 4 would increase the oxygen vacancy concentration, enhance oxygen diffusion, and increase the corrosion rate.

This present work showed that tin is uniformly distributed in the metal and hence may become a part of the ZrO_2 lattice without a diffusion process.

It was demonstrated that tin is uniformly distributed in the oxide. Considerations of ionic radii would indicate that tin should be incorporated substitutionally in the oxide film, in which case it would have a valence of three. This would increase the oxygen ion vacancies and enhance corrosion. Tin, in fact, does tend to increase the corrosion rate of zirconium.

In contrast to tin, the concentrations of iron, nickel, and chromium in the metal are very low except in localized areas of intermetallic enrichment. Thus, in order to dissolve evenly in the oxide film, these elements would have to diffuse through considerable distances in the oxide lattice.

This present work indicated that the Fe-Ni-rich aggregate was, in fact, able to dissolve and diffuse homogeneously in the oxide in the cold-worked and alpha-annealed material in which the precipitate was very finely dispersed. The corrosion resistance of this material was superior to that of the

material heat treated to form a coarse distribution of intermetallics in the metal. The enhanced corrosion resistance apparently associated with the dissolution of iron and nickel in the oxide suggests that these elements dissolved interstitially in the oxide.

In contrast to the iron-nickel aggregate, the iron-chromium aggregate did not appear to dissolve in the oxide even when finely distributed in the metal. To account for this it may be suggested that a very thin layer of Cr_2O_3 formed at the surface of the intermetallic particle in the oxide, and acted as a barrier to diffusion of chromium. The beneficial effect of chromium on the corrosion resistance of iron is believed to be based on a similar mechanism.

At low temperatures, the diffusion of oxygen through the film may depend upon the properties of the oxide subgrain boundaries rather than on the bulk structure. If this is so, the addition of even very small concentrations of alloying elements at the right places could have a large effect on the corrosion rate. Properly located, these alloying additions could affect the degree of disorder in the subgrain boundaries as well as the size of the subgrains (and hence their number). Our observation that iron and nickel dissolve in the oxide film while chromium does not, indicates the possibility that the former two elements may contribute to such a corrosion mechanism.

2. Niobium-Copper Alloys

Analysis of the oxide film on the beta-quenched and tempered sample indicated that niobium was homogeneously distributed in the oxide. The niobium-rich areas in the metal are extremely fine; if they exist in the oxide with similar dimensions they would be impossible to detect with the microprobe. Hence, the data obtained in this study do not permit us to determine whether the niobium in the oxide film is concentrated in discrete regions or uniformly distributed. However, Dalgaard has noted that in this condition of heat treatment, increasing the niobium content from 0.5 to 7 wt % has little or no effect on the oxidation resistance of the system. This is a strong indication that if niobium particles do exist in the oxide they are of minor importance in the corrosion mechanism.

The alternative possibility that niobium dissolves in the oxide film appears more plausible. The ionic radii of niobium and zirconium are such that niobium may be incorporated in the zirconium oxide either interstitially or

substitutionally. The fact that small additions of niobium tend to increase the corrosion rate of zirconium[8] would suggest that niobium has entered the oxide film substitutionally.

The behavior of copper in these alloys was somewhat different from that of niobium. Although the copper distributed rather uniformly in both the alloy and the oxide in the beta-quenched and tempered sample, it showed lack of homogeneity in both alloy and oxide of the beta-annealed specimen. It is thus reasonable to suspect that copper does not diffuse readily in the oxide lattice during corrosion.

An additional effect was noted with copper. In the beta-quenched and tempered sample, copper accumulated at the metal-oxide interface. A high copper concentration could act as a diffusion barrier to one or more of the participants in the corrosion reaction. The importance of such a layer to the control of oxidation, and perhaps hydriding, of zirconium alloys could be significant.

3. Nickel Alloy

Microprobe data showed that in the Zr - 1 wt % Ni alloy the nickel is distributed homogeneously, but at a low level, in the oxide film. This apparent solution of nickel in the oxide is similar to that observed in nickel-bearing Zr-2. It occurred despite a rather coarse distribution of nickel-rich areas in the metal. Considerations of ionic radii, together with the fact that nickel enhances the corrosion resistance of zirconium under the conditions used on this sample,[10] indicate that nickel is incorporated interstitially in the oxide lattice.

Nickel accumulated to a striking degree at the metal-oxide interface. Again, such a layer could serve as an effective barrier to either oxygen or zirconium diffusion and hence reduce the corrosion rate of zirconium alloys. It may be noted that nickel additions in excess of those required to alter the diffusional properties of the oxide enhance the corrosion resistance of zirconium[8,9]. This lends credence to the existence of a nickel-rich band, because the effectiveness of this band should be improved by increased amounts of nickel made available from the metal.

ACKNOWLEDGMENT

The assistance of Dr. Sven B. Dalgaard, AECL, is warmly appreciated. His suggestions aided materially in the metallurgical phases of the work.

BIBLIOGRAPHY

1. Lustman, B. and F. Kerze, Jr., eds. The Metallurgy of Zirconium. National Nuclear Energy Series, Division VII, Volume 4. McGraw-Hill Book Co., Inc., 1955.

2. Rubenstein, L. S., J. G. Goodwin, and F. L. Shubert. "Relationship of Cooling Rate to the Corrosion Resistance of Zircaloy-2." Bettis Technical Review, Westinghouse Electric Corp., WAPD-BT-10, p. 23 (October 1958).

3. Oestberg, G., "Determination of the Composition of the Second Phase in Zircaloy." J. Nucl. Mater. 7, 103-106 (1962). Atkiebolaget Atomenergi, Stockholm.

4. Kirianenko, A. and F. Maurice. "Microanalyseur a sonde electronique. Dispositif de balayage lineaire," Report CEA-2291, 5 (1963), Commissariat a l'Energie Atomique. Centre d'Etudes Nucleaires, Saclay.

5. Dalgaard, S. B. Corrosion and Hydriding Behavior of Some Zr 2.5 wt % Nb Alloys in Water, Steam, and Various Gases at High Temperature. Atomic Energy of Canada Ltd., Chalk River, Ont. Report AECL-1513 (1962).

6. Britton, C. F. and J. N. Wanklyn. "The Resistance of Zirconium and Its Alloys to High Temperature Water." AERE-M/R-1924. United Kingdom Atomic Energy Authority, Research Group. AERE, Harwell, Berks, England (1956).

7. Cox, B. "Oxidation and Corrosion of Zirconium and Its Alloys (Oxide Film Breakdown in Arc-Melted Sponge Zirconium)." AERE-R-2874 (March 1959). Also Corrosion 16, 380t-4t (August 1960).

8. Porte, H. A., J. G. Schnizlein, R. C. Vogel, and D. F. Fischer. "Oxidation of Zirconium and Zirconium Alloys." Argonne National Laboratory, Lemont, Ill. USAEC Report, ANL-6046 (September 1959).

9. Pemsler, J. P. The Corrosion of Zirconium Alloys in 900°F Steam. Nuclear Metals, Inc., Cambridge, Mass. USAEC Report NMI-1208 (August 1958).

250X

a. OXIDIZED Zr-2, MOUNTED IN BAKELITE. Note excessive rounding of the specimen edge and the poor contact between oxide and mounting medium due to shrinkage of the Bakelite.

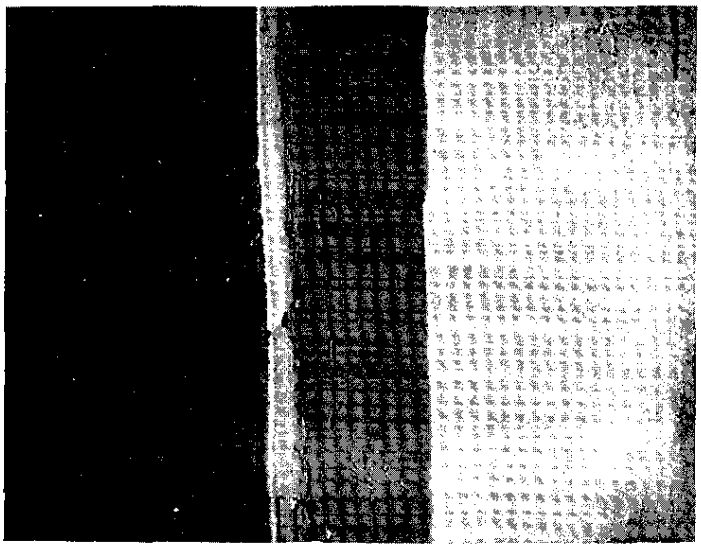

250X

b. OXIDIZED Zr-2, MOUNTED IN DIALLYLPHTHALATE. Note little edge rounding; mounting medium has adhered well to the oxide.

FIG. 1 METALLOGRAPHIC MOUNTING TECHNIQUE FOR SECURING MAXIMUM SPECIMEN FLATNESS

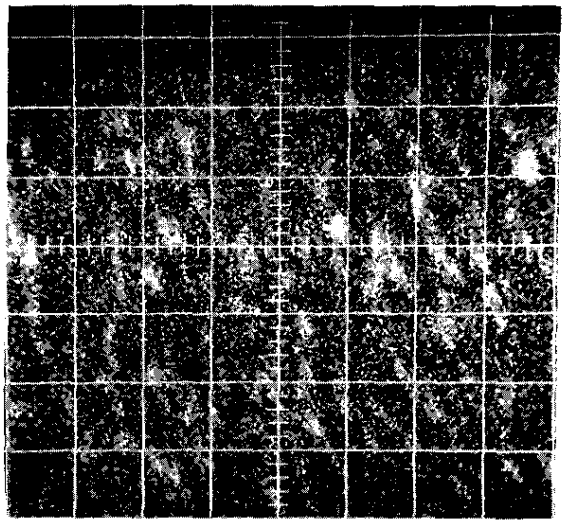

400X

a. UNCOATED SPECIMEN. Poor resolution due to beam instability.

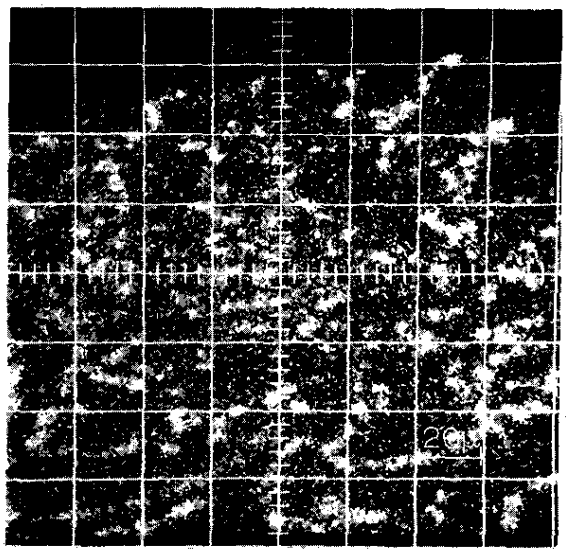

400X

b. SPECIMEN COATED WITH ALUMINUM TO STABILIZE BEAM POSITION.

FIG. 2 IRON X-RAY AREA SCAN OF COATED AND UNCOATED ZIRCALOY-2. Areas rich in iron are shaded light.

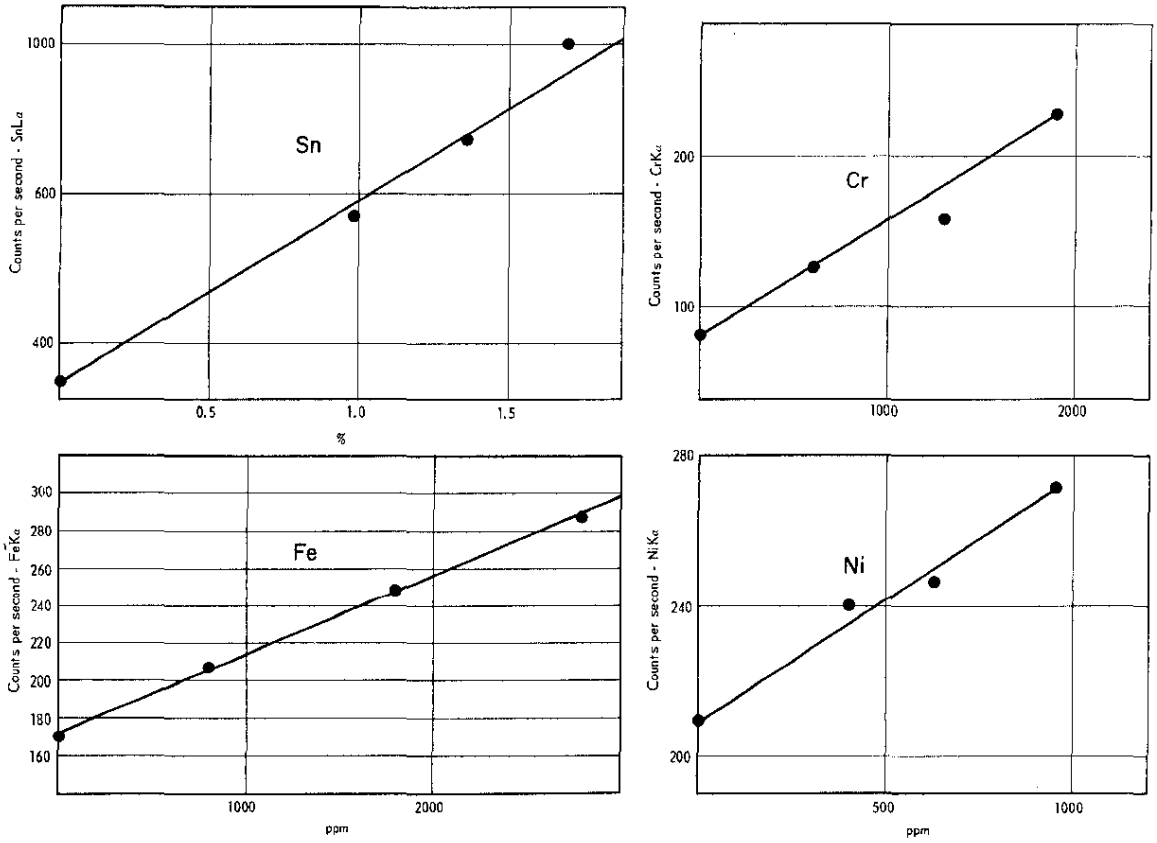

FIG. 3 STANDARD CURVES FOR ALLOYING ELEMENTS IN ZIRCALOY-2

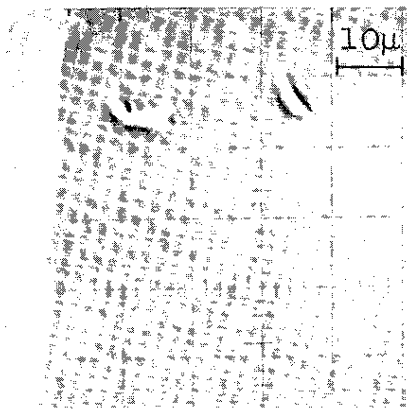

800X

a. TARGET CURRENT IMAGE

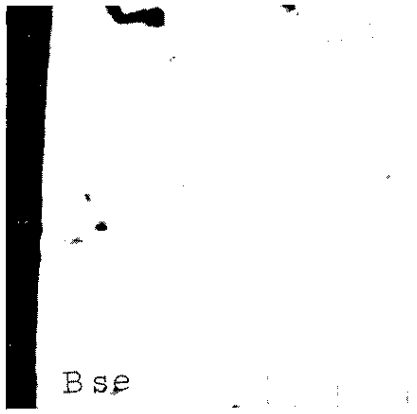

800X

b. ELECTRON BACKSCATTER IMAGE

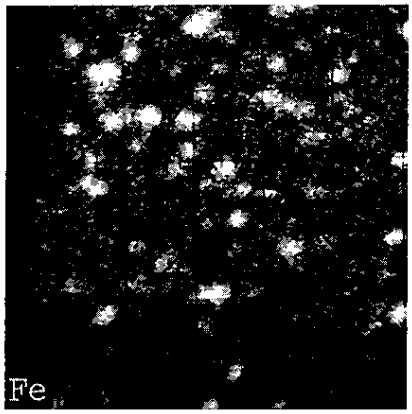

800X

c. Fe X-RAY IMAGE

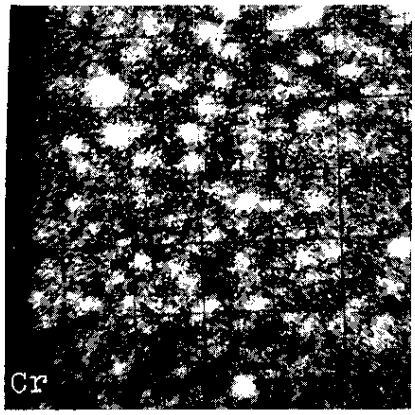

800X

d. Cr X-RAY IMAGE

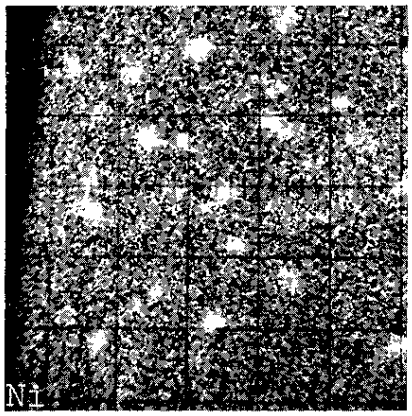

800X

e. Ni X-RAY IMAGE

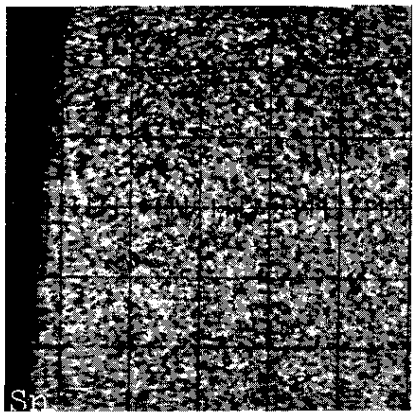

800X

f. Sn X-RAY IMAGE

FIG. 4 X-RAY AREA SCANS OF ALPHA-ANNEALED ZIRCALOY-2.
Specimen no. J-3930

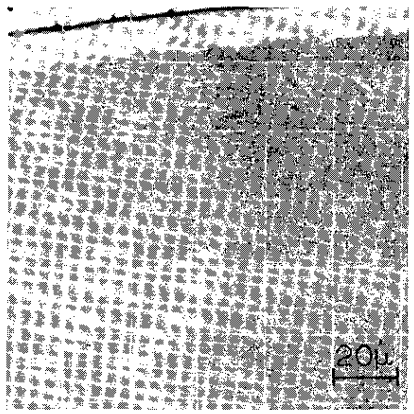

400X

a. TARGET CURRENT IMAGE. The oxide coating (gray layer) is visible.

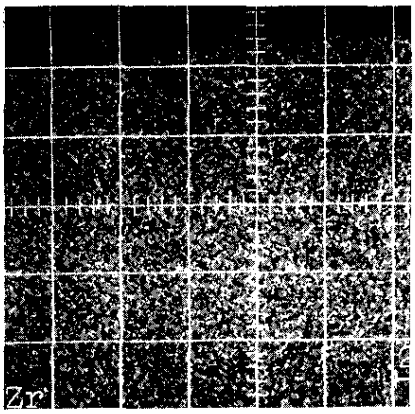

400X

b. Zr X-RAY IMAGE

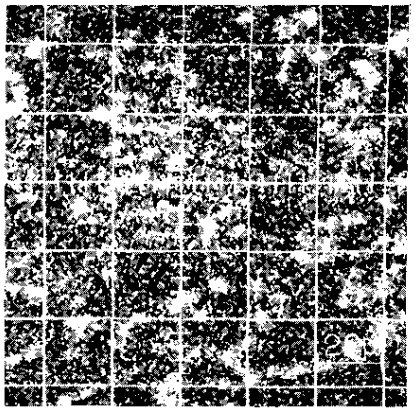

400X

c. Fe X-RAY IMAGE

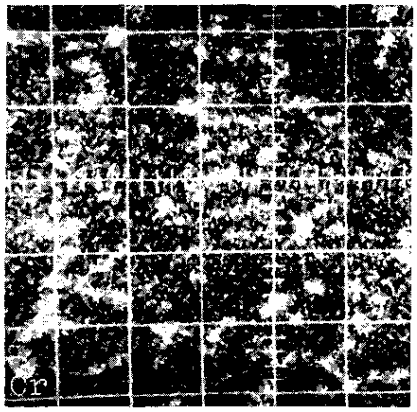

400X

d. Cr X-RAY IMAGE

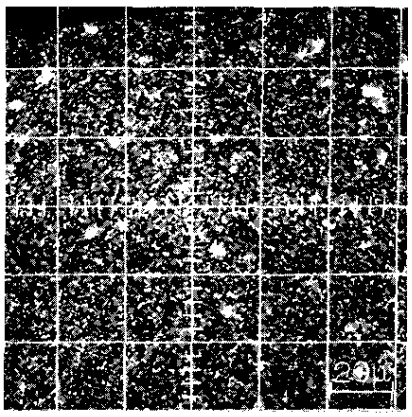

400X

e. Ni X-RAY IMAGE

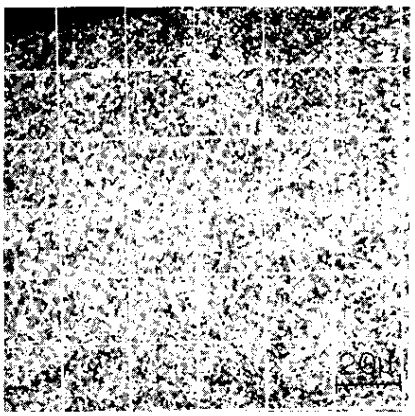

400X

f. Sn X-RAY IMAGE

FIG. 5 X-RAY AREA SCANS OF ALPHA-ANNEALED ZIRCALOY-2.
Specimen no. C03

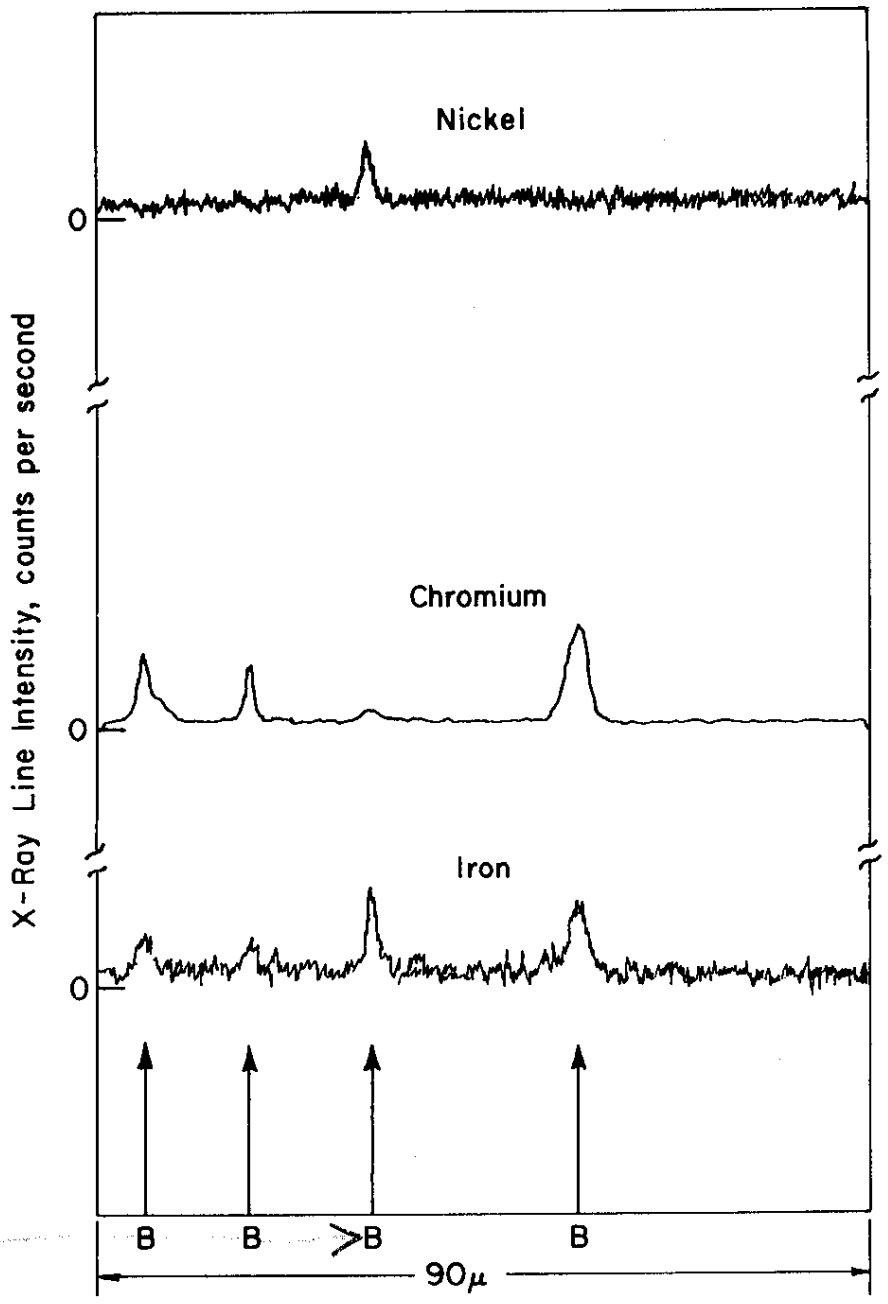

FIG. 6-a LINE SCANS OF ALLOYING ELEMENTS IN ALPHA-ANNEALED ZIRCALOY-2. Specimen no. C03

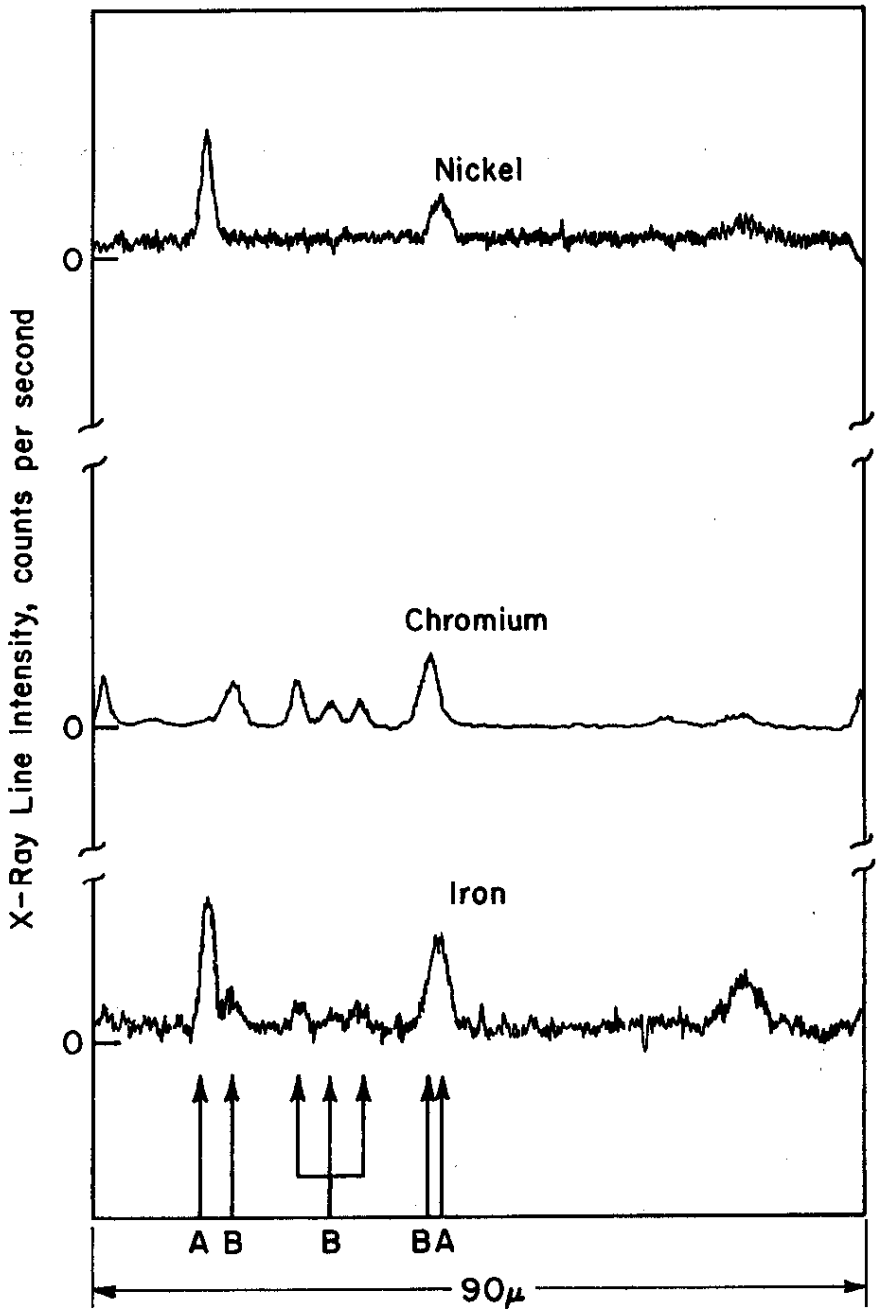

FIG. 6-b LINE SCANS OF ALLOYING ELEMENTS IN ALPHA-ANNEALED ZIRCALOY-2. Specimen no. C03

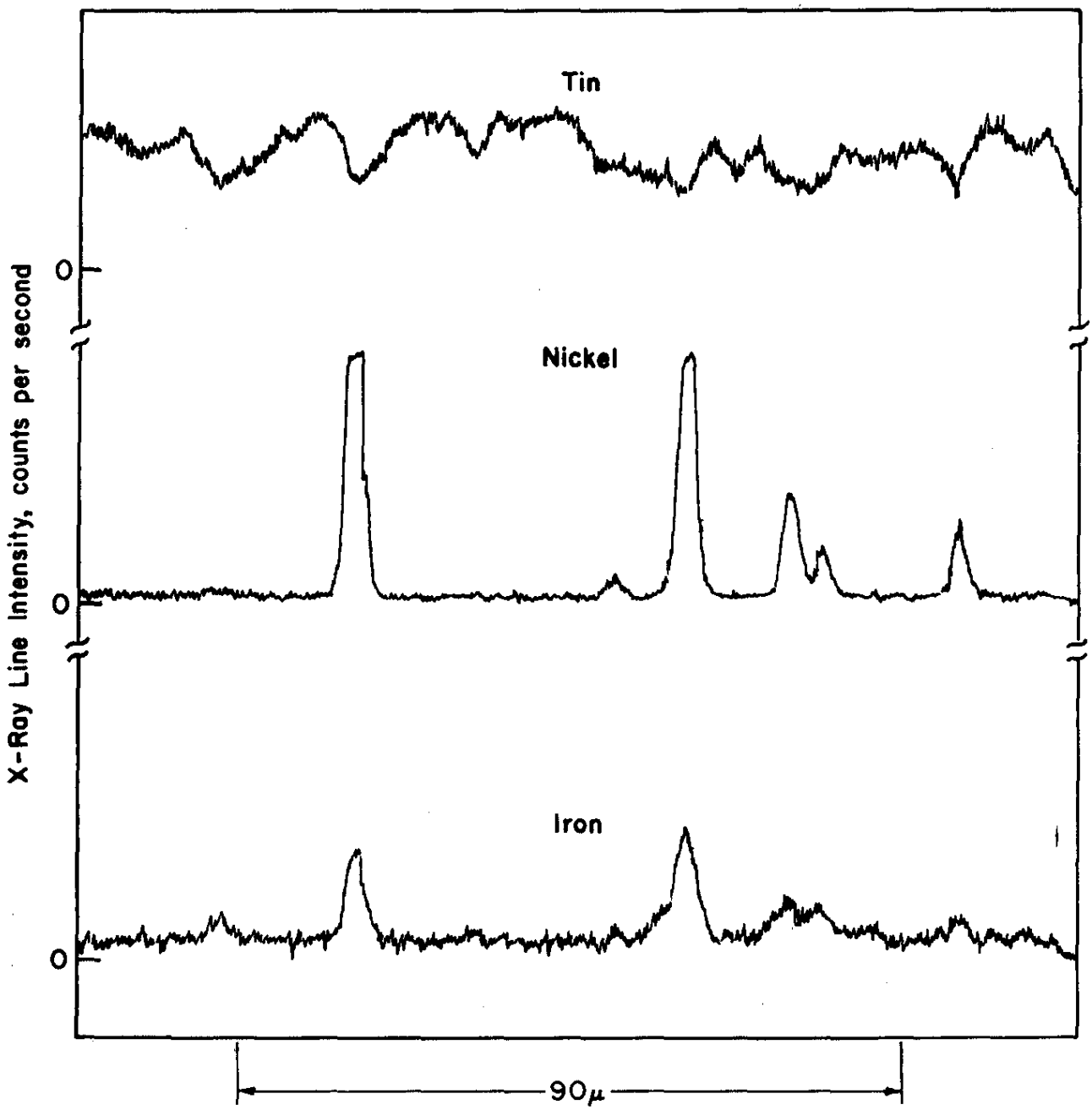

FIG. 6-c LINE SCANS OF ALLOYING ELEMENTS IN ALPHA-ANNEALED ZIRCALOY-2. Specimen no. C03

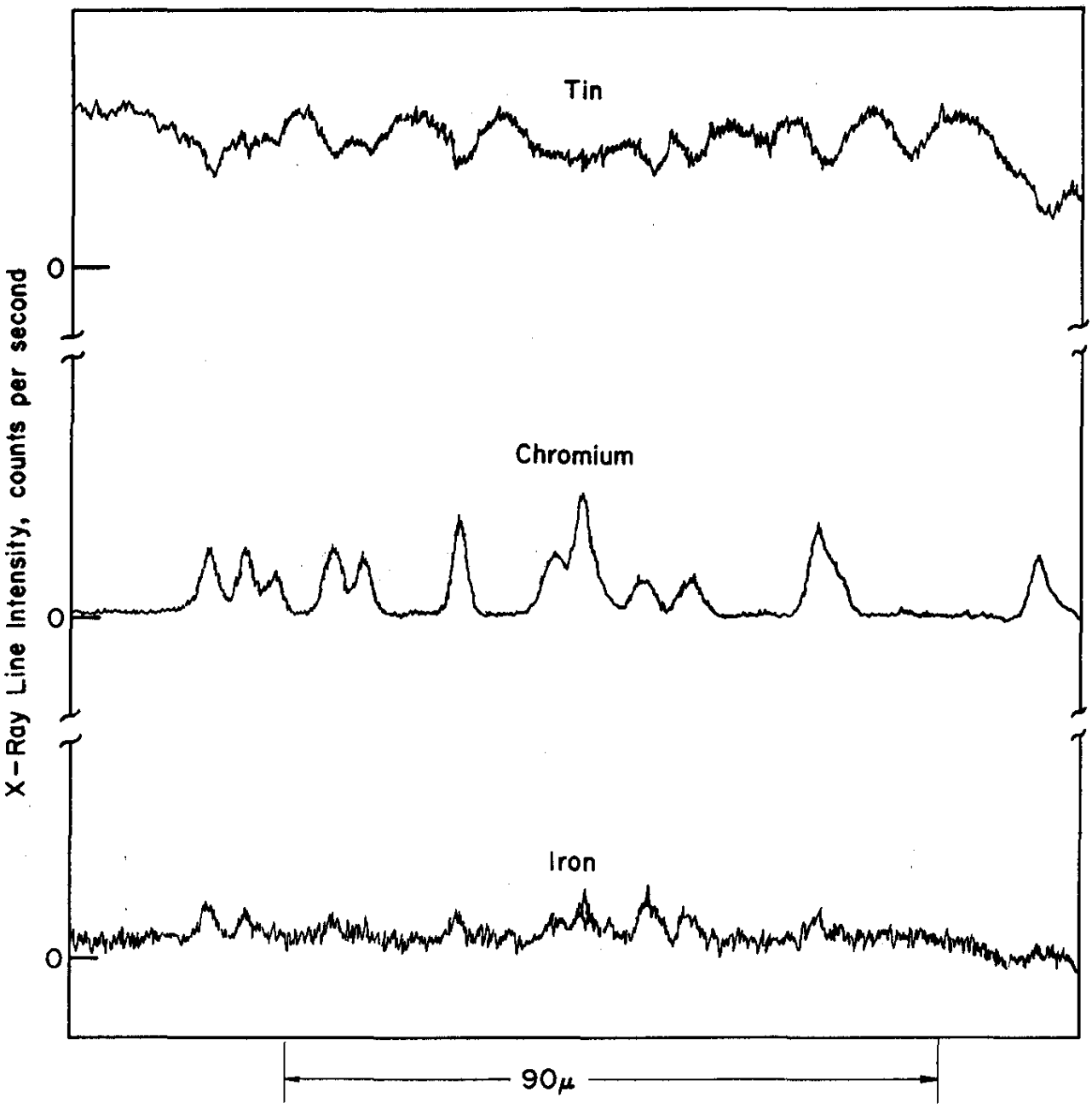

FIG. 6-d LINE SCANS OF ALLOYING ELEMENTS IN ALPHA-ANNEALED ZIRCALOY-2. Specimen no. C03

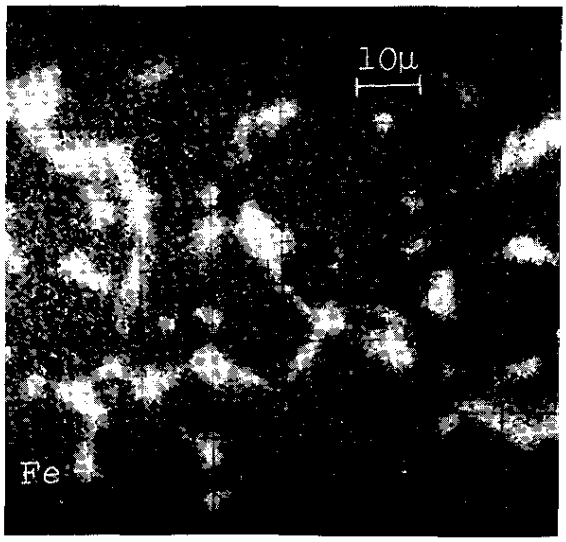

800X

a. Fe X-RAY IMAGE

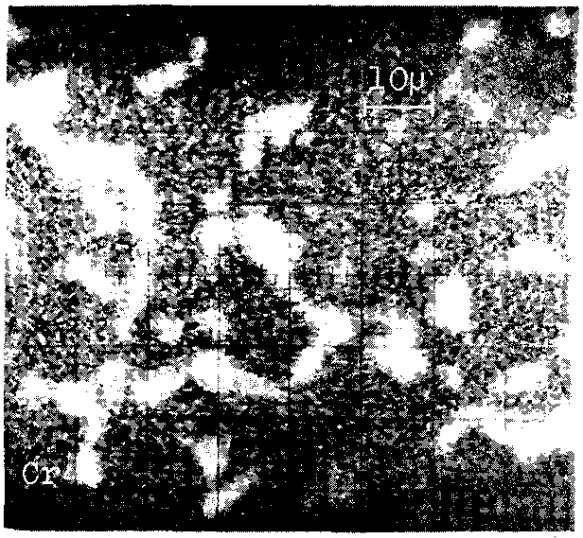

800X

b. Cr X-RAY IMAGE

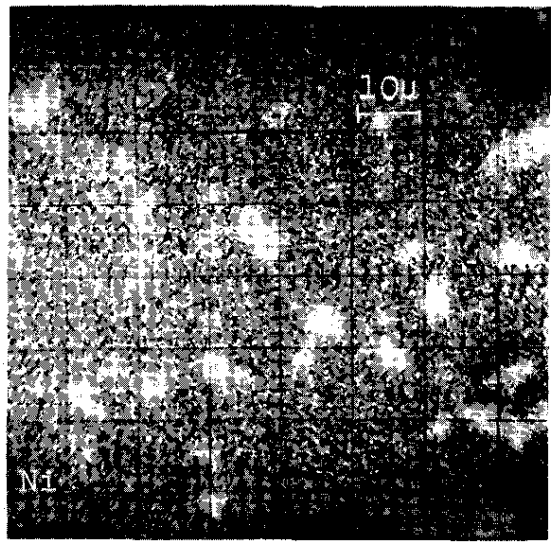

800X

c. Ni X-RAY IMAGE

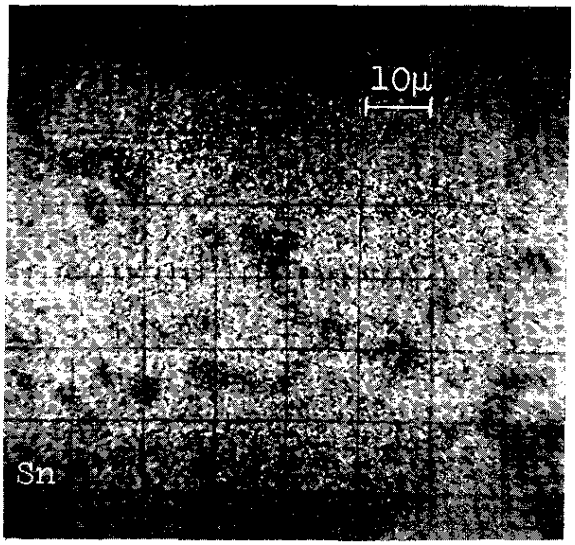

800X

d. Sn X-RAY IMAGE

FIG. 7 X-RAY AREA SCANS OF ALPHA AND BETA-ANNEALED ZIRCALOY-2. Specimen no. J-7871

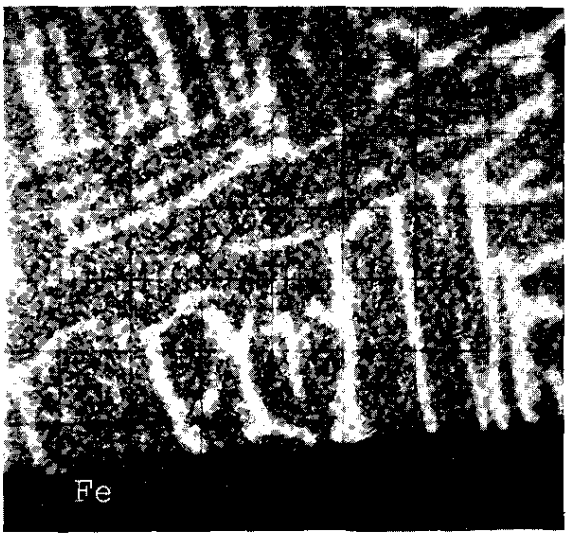

400X

a. Fe X-RAY IMAGE

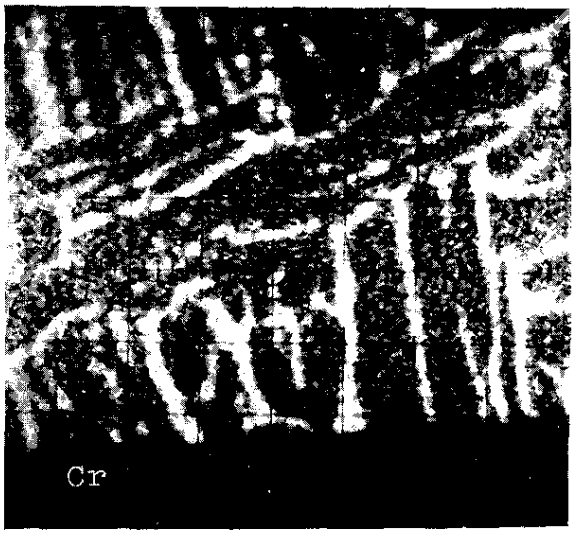

400X

b. Cr X-RAY IMAGE

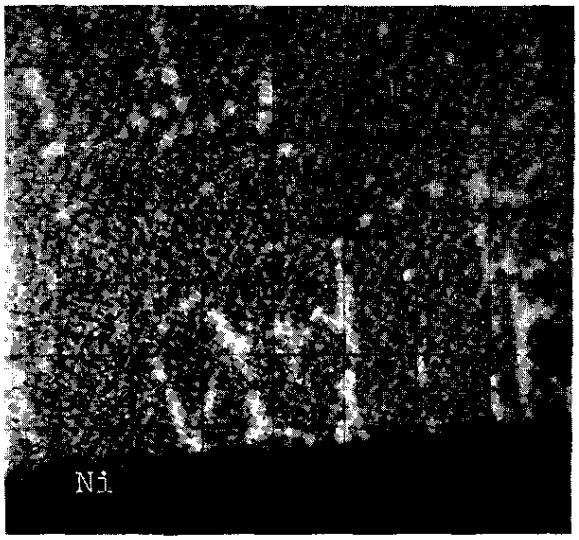

400X

c. Ni X-RAY IMAGE

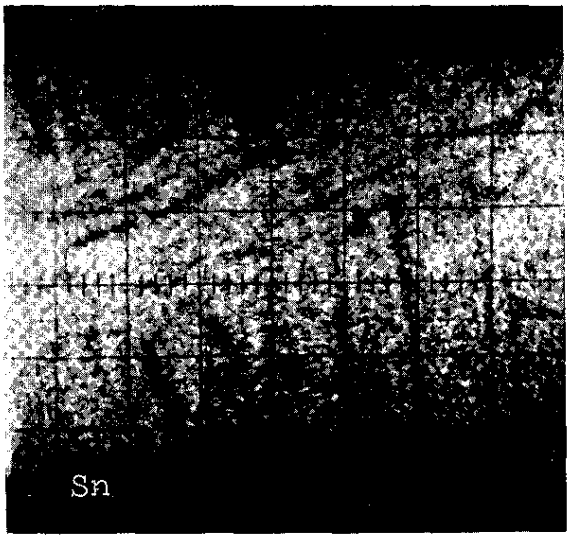

400X

d. Sn X-RAY IMAGE

FIG. 8 X-RAY AREA SCANS OF BETA-ANNEALED ZIRCALOY-2.
Specimen No. J-3960

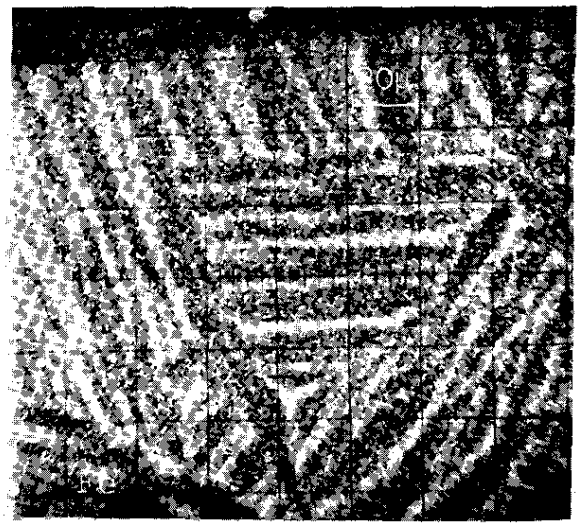

400X

a. Fe X-RAY IMAGE

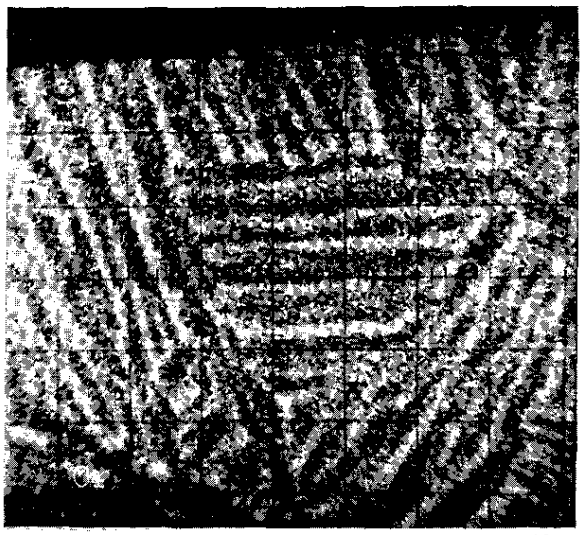

400X

b. Cr X-RAY IMAGE

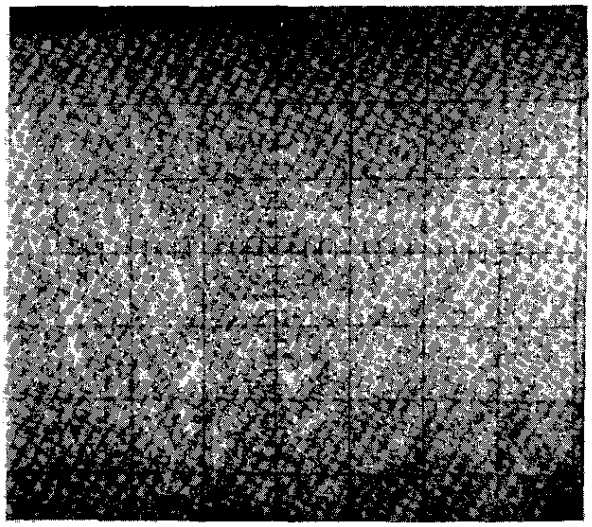

400X

c. Ni X-RAY IMAGE

FIG. 9 X-RAY AREA SCANS OF BETA-QUENCHED ZIRCALOY-2.
Specimen No. L-1195

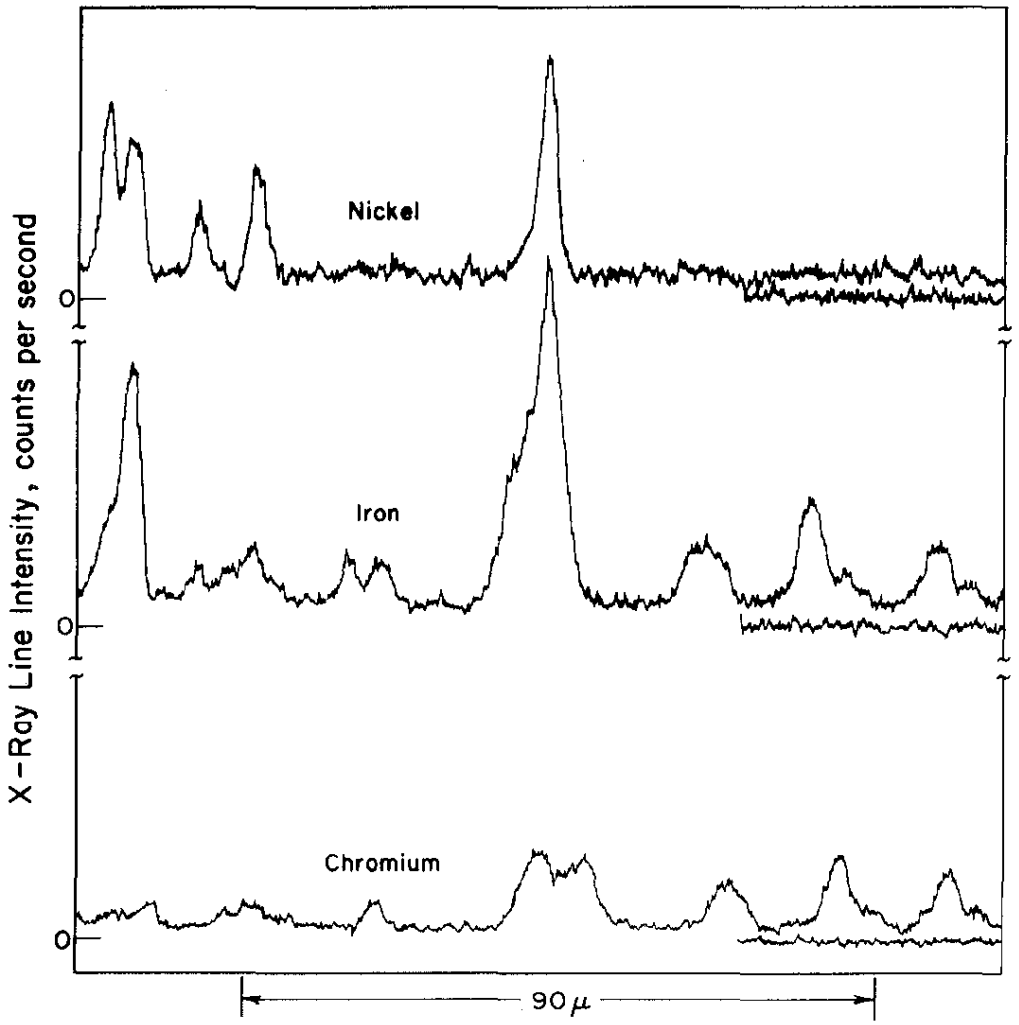

a. METAL

FIG. 10 LINE SCANS OF ALPHA-ANNEALED ZIRCALOY-2 AND ITS CORROSION OXIDE. Specimen No. C03

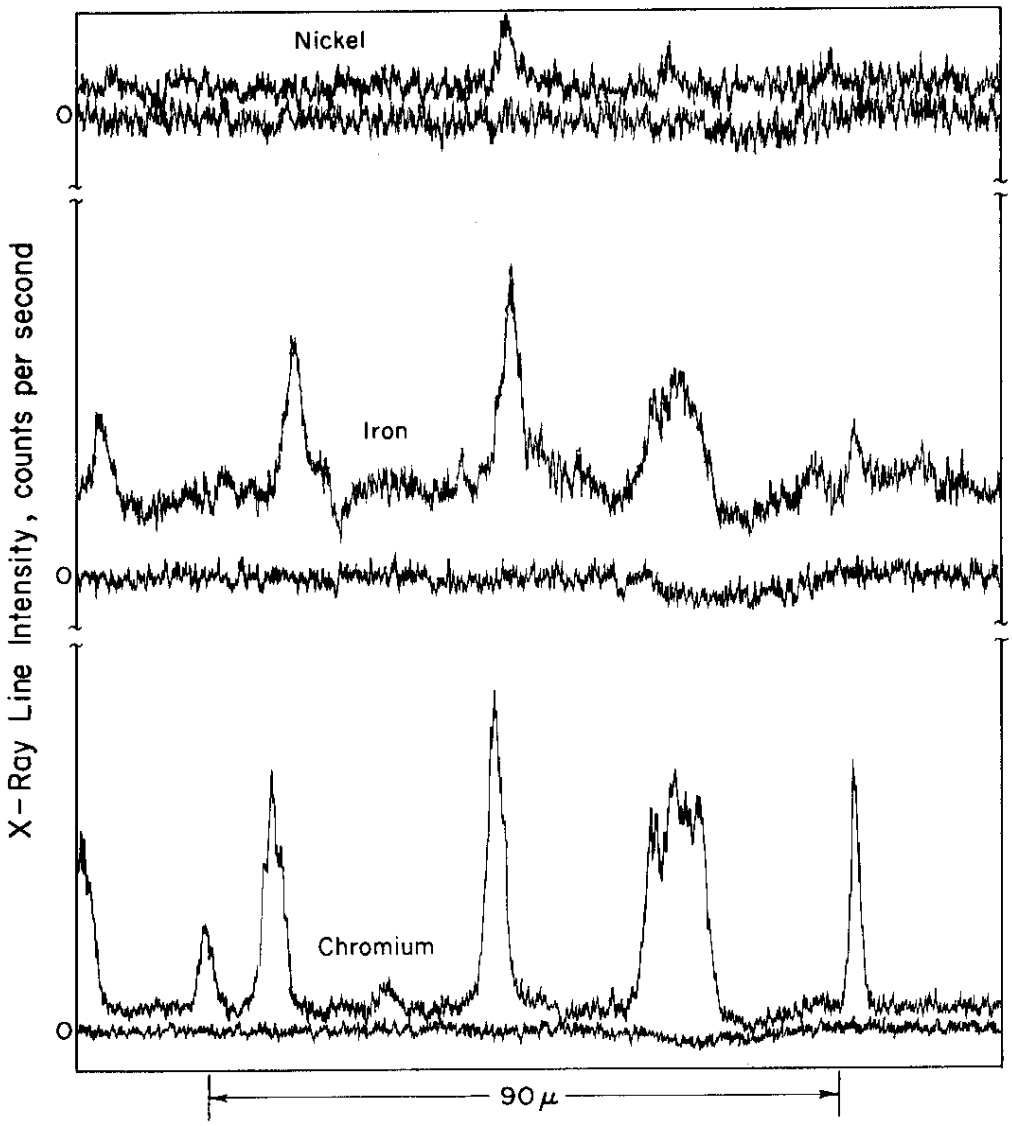

b. SCANS IN OXIDE PARALLEL TO SURFACE

FIG. 10 LINE SCANS OF ALPHA-ANNEALED ZIRCALOY-2 AND ITS CORROSION OXIDE. Specimen No. C03

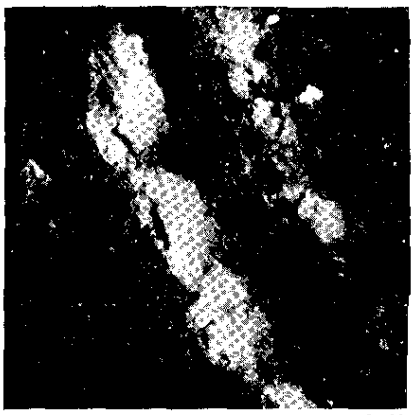

125X

Stringers with Cracking White Oxide

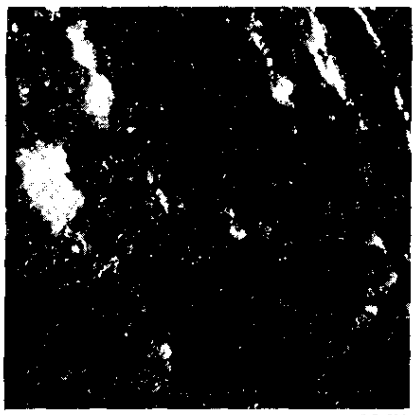

125X

Stringers, Oxide-filled and Empty

a. MICROGRAPHS OF TYPICAL STRINGERS IN PLANE OF SPECIMEN. OBLIQUE ILLIMINATION.

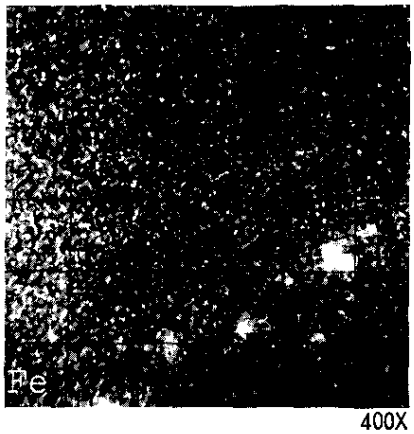

400X

Fe X-RAY IMAGE

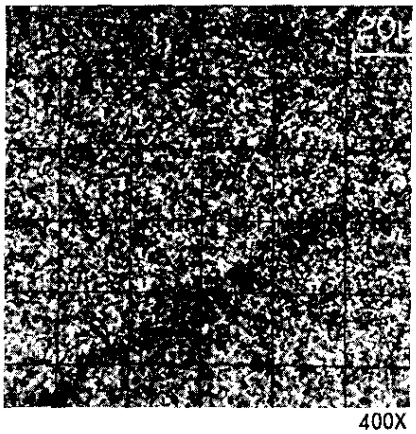

400X

Zr X-RAY IMAGE

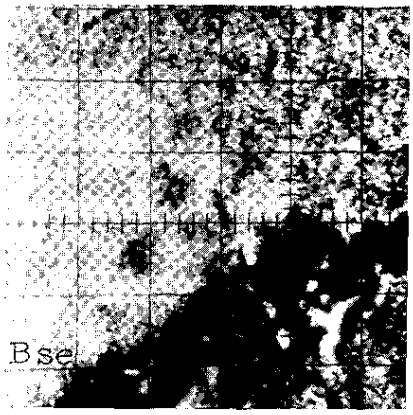

400X

BACKSCATTER IMAGE

b. AREA SCANS OF SAME AREA.

FIG. 11 COMPARISON OF METALLOGRAPHIC AND MICROPROBE STRUCTURES OF STRINGERS ON SURFACES OF AUTOCLAVED ZIRCALOY-2.
Specimen no. WC-60

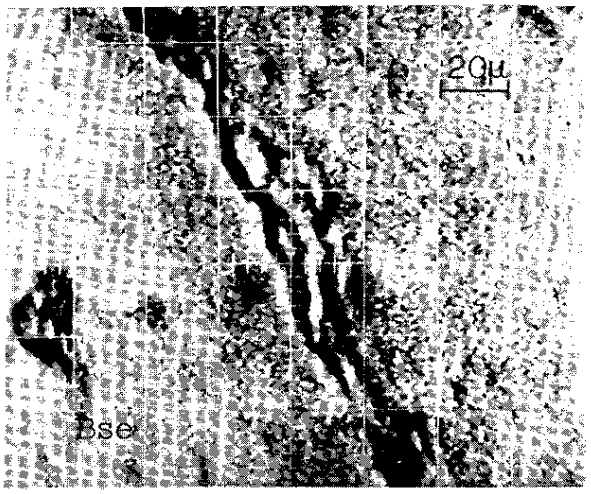

400X

a. ELECTRON BACKSCATTER IMAGE

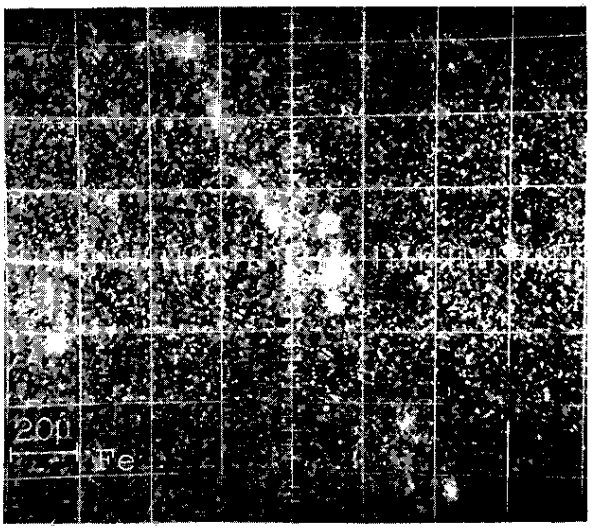

400X

b. Fe X-RAY IMAGE

FIG. 12 X-RAY AREA SCANS OF STRINGERS IN OXIDE COATING. Specimen no. WC-63.

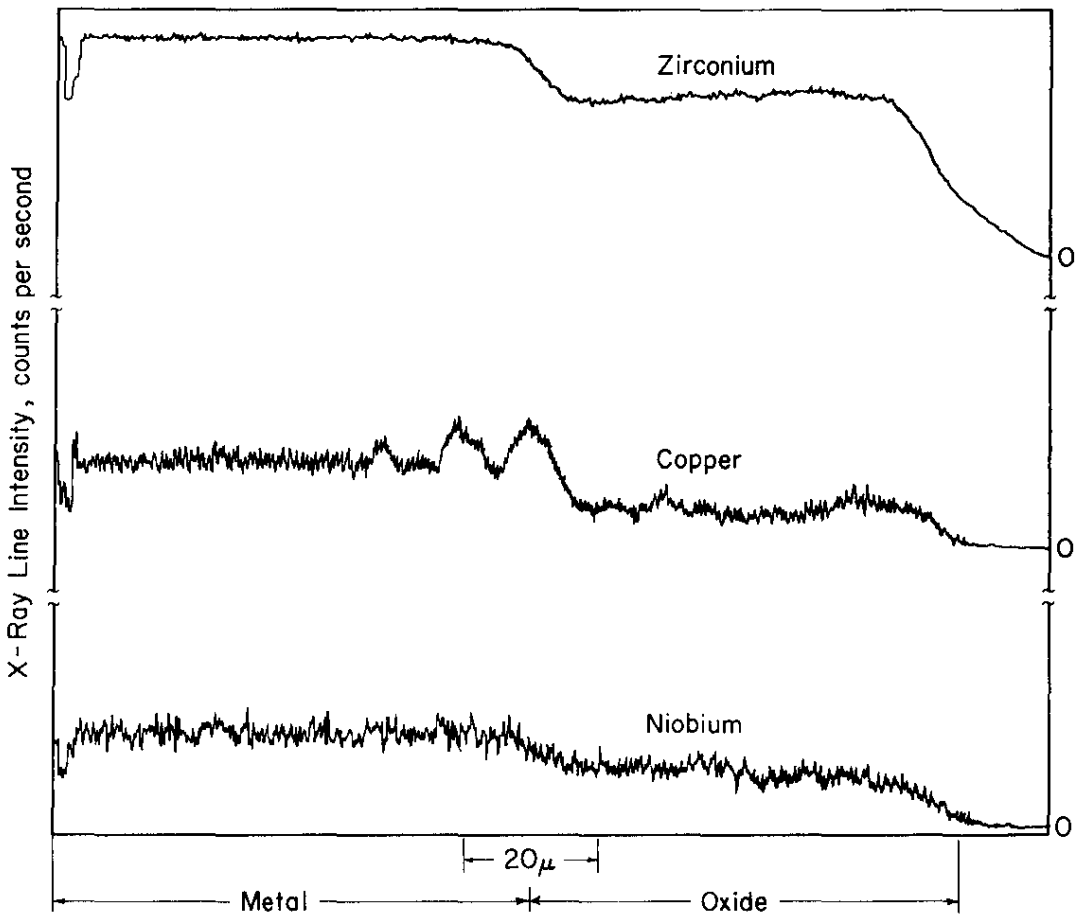

FIG. 13 LINE SCANS OF BETA-QUENCHED AND TEMPERED Zr-Nb-Cu ALLOY.
Specimen No. B-246

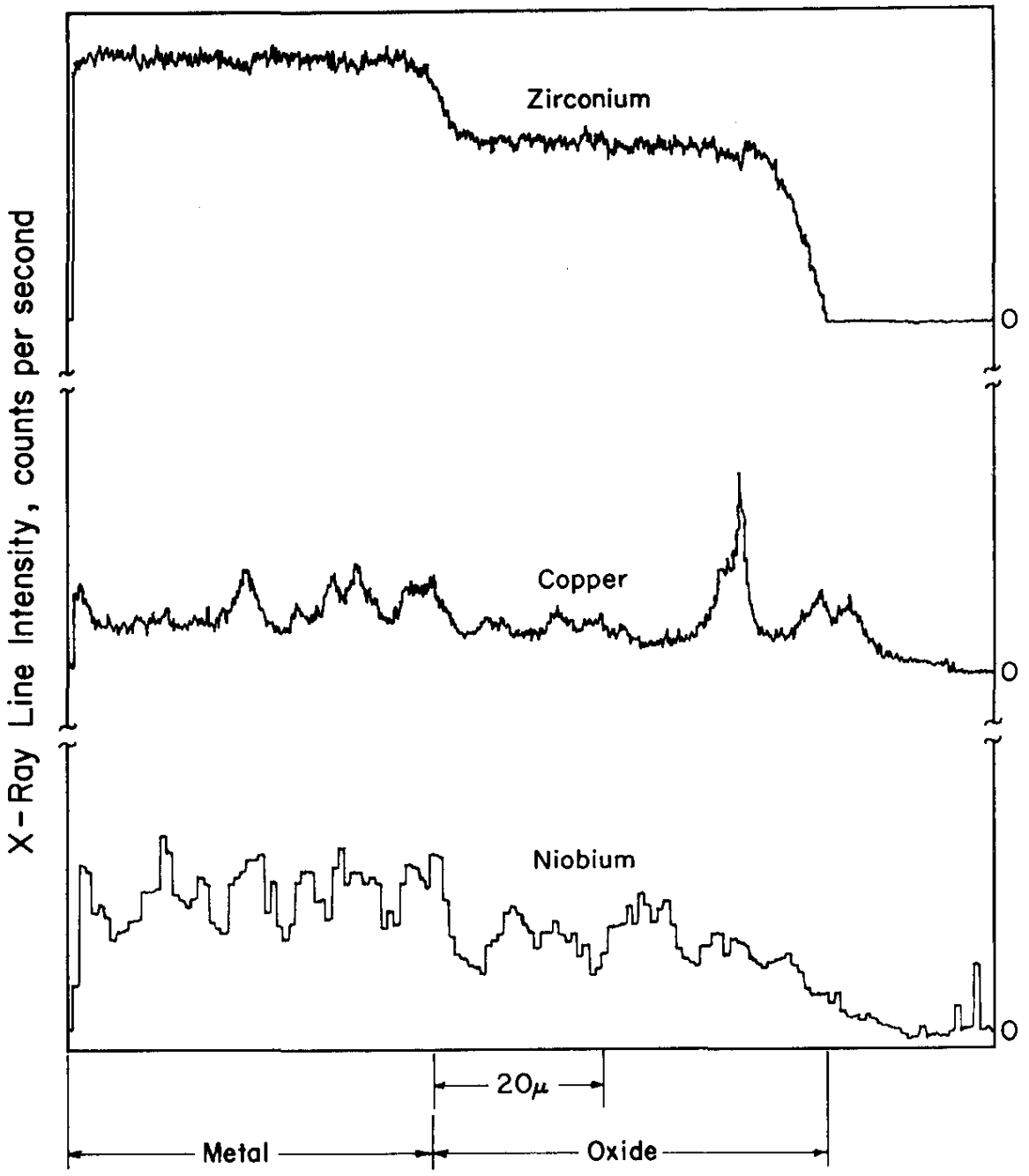

FIG. 14 LINE SCANS OF ALPHA PLUS BETA-ANNEALED Zr-Nb-Cu ALLOY.
Specimen No. B-179

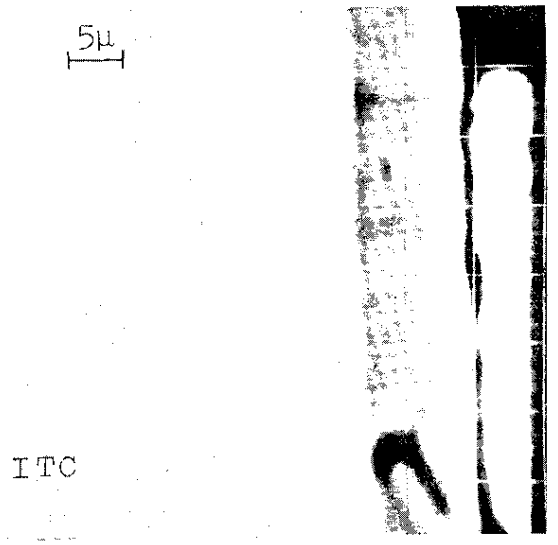

~1600X

a. INVERTED TARGET CURRENT IMAGE

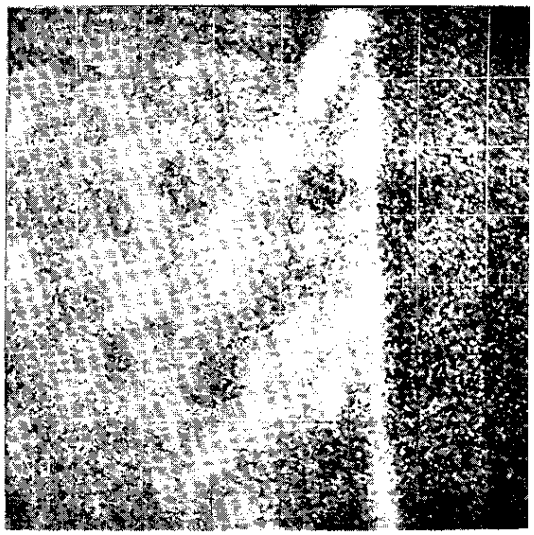

~1600X

b. Ni X-RAY IMAGE

FIG. 15 X-RAY AREA SCANS OF ZIRCONIUM-1 wt % NICKEL ALLOY.
Specimen no. 153-B.

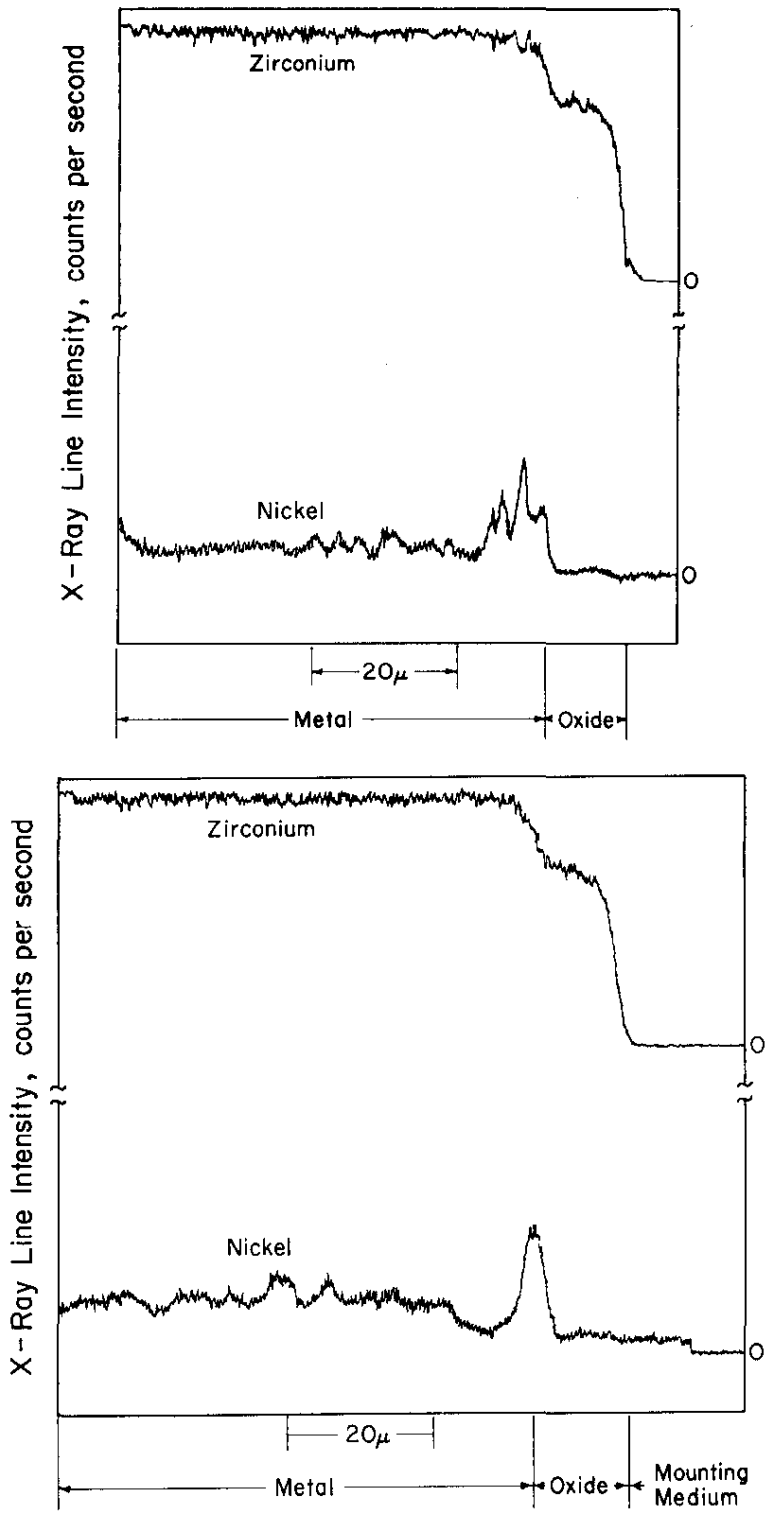

FIG. 16 LINE SCANS OF ZIRCONIUM-1 wt % NICKEL ALLOY.
Two Different Areas of Specimen no. 153-B.

TABLE I

Comparison of Standard Analytical
and Microprobe Analyses of Zirconium Alloys

Element, ppm	Standard No. EZ-7		Standard No. EZ-8		Standard No. EZ-10		"Pure" Zr
	Standard Analytical	Micro. probe	Standard Analytical	Micro-probe	Standard Analytical	Micro-probe	Microprobe
Fe	800 ±13	850	1800 ±10	1860	2800 ±35	2750	-50
Cr	600 ±8	730	1300 ±12	1140	1900 ±29	1930	180
Ni	400 ±9	470	620 ±12	560	950 ±10	950	160
Sn(a)	0.98 ±0.01	0.92	1.36 ±0.01	1.33	1.70 ±0.02	1.85	0.0
Ti	52 ±1.5		62 ±1		125 ±4		
Si	48 ±3		154 ±2		235 ±2		
B	0.19 ±0.02		0.55 ±0.03		0.83 ±0.02		
Cu	27 ±1		64 ±2		112 ±1		
Mn	17 ±2		28 ±0		52 ±2		
Co	17 ±2		28 ±1		52 ±1		
V	24 ±3		52 ±1		98 ±1		
Al	23 ±1		39 ±2		81 ±3		
Mo	20 ±7		60 ±3		94 ±1		
Pb	22 ±2		50 ±4		175 ±5		

(a) Expressed as %.

TABLE II

Description of Zircaloy-2 Specimens

Sample Number	Source	Ingot	Heat Treatment Hr	Heat Treatment °C	Metallurgical Structure	Test Days	Test °C	Wt gain, mg/dm²	Relative Corrosion Resistance	Microprobe Analyses Ni, ppm	Fe, ppm	Cr, ppm	Sn, %
WC-60	AECL[a]				α-annealed	352	360	128		530	1160	1000	1.40
WC-63	AECL[a]					360	316	30		510	1100	930	1.50
C03	AECL					552	360	205		530	1400	1250	1.35
J-3930	BAPL	D2	4	750		7	400	14	Excellent	460	1300	950	1.40
J-3932	BAPL	D2	4	750		28	400	29	Good	540	1600	900	1.40
J-7871	BAPL	K527	2	843	α + β annealed	98	400	159	Poor	600	1400	750	1.30
J-3960	BAPL	D2	1/4 Slow-cooled	1050	β-annealed	7	400	23	Good	650	1300	1400	1.40
L-1195	BAPL	D2	1/4 Quenched	1050	β-quenched	7	360	17	Fair	600	1500	950	1.30

(a) Ingot analysis for WC samples shown in Table III.

TABLE III

Chemical Analyses of Zirconium Alloys

Constituent	Concentration, ppm	
	Zircaloy-2 (WC-60 and WC-63)	Zr-2.5 wt % Nb-0.5 wt % Cu
Al	50	35
B	<0.2	<0.2
C	<30	70-90
Ca	<30	-
Cd	<0.5	<0.3
Co	<5	<5
Cr	970	78-94
Cu	<20	4,800-5,300
Fe	940	800-890
H	22	4
Hf	84	48
Mg	<10	<10
Mn	<10	<10
N	45	21-30
Na	<20	-
Nb	-	25,000-25,500
Ni	430	<10
O	980	1,000-1,200
Pb	15	<5
Si	60	86-98
Sn	15,000	<10
Ti	<10	<20
U	<5	0.7
V	<5	<5
W	<50	<25
Zn	-	<50

TABLE IV

Concentrations of Alloying Elements in Zr-2
Outside the Zones of Local Enrichment, ppm
Specimen No. J-3932

Element	Bulk Concentration	Concentration in Matrix	
		Average of Four Regions	Estimated Standard Deviation
Fe	1600	400	120
Ni	540	215	60
Cr	900	200	25